Mapping Rydberg States of H_2 with the Halfium R-Matrix Method

Rawand MEZLINI[1,2], Soumaya BEZZAOUIA[1], David HVIZDOS[2], Chris. H. GREENE[3], Christian JUNGEN[4], Ioan F. SCHNEIDER[2], Mourad TELMINI[1]*

[1] *LSAMA, Department of Physics, Faculty of Science of Tunis, University of Tunis El Manar, 2092 Tunis, Tunisia*
[2] *LOMC, UMR 6294 CNRS and Université Le Havre Normandie, 25 rue Philippe Lebon, BP 540, 76058 Le Havre, France*
[3] *Department of Physics and Astronomy, Purdue University, West Lafayette, Indiana 47907, USA*
[4] *LAC CNRS-FRE2038, Université Paris-Saclay, ENS Cachan, Campus d'Orsay, Bat. 505, 91405 Orsay, France*

(Received 28 August 2025 / Accepted 6 November 2025)

In this paper, we use the Halfium *R*-matrix method to investigate the Rydberg states of the H_2 molecule up to $n = 20$, filling the gap above the low-lying bound states already calculated with configuration interaction packages. Moreover, we show that the use of Quantum Defect Theory scaling laws, allows for a comprehensive analysis of the regular patterns resulting from the coupling between Rydberg series and doubly excited states. The results should open the door for more efficient quasi-diabatization of the potential energy curves which is required for calculating cross sections and rate coefficients of the ($e + H_2^+$) collisional processes, involved in the plasma modeling for fusion devices.

Keywords: Rydberg states, Halfium R-matrix method, spectroscopy, dissociative recombination, molecular hydrogen, quantum defect theory, electron-molecule collisions, divertor region

DOI: 10.1585/pfr.21.2401009

1. Introduction

Rydberg states of molecular hydrogen are well known to play a crucial role in collisional processes involving low-energy electrons and H_2^+ ions. Indeed, they are responsible for the complex resonance structures appearing in both the (Ro) Vibrational Excitation (RVE) and Dissociative Recombination (DR) cross sections of the ($e + H_2^+$) collision. In fact, the indirect DR process—in which the electron is first captured in a ro-vibrational level of a Rydberg state of the neutral molecule, before going to pre-dissociation through the coupling with the doubly excited dissociative states—can even be dominant and thus entirely necessary to correctly determine the total rate for neutralization of Hydrogen plasma.

The hydrogen molecule, despite being the simplest molecule in nature, hides a rich and intricate quantum landscape. Achieving an ab initio precise description of its highly excited states—especially the Rydberg manifold—is crucial because these states are the gateways through which electrons recombine. Accordingly, Rydberg states of H_2 have attracted the attention of several pioneering theoreticians. Early work by Giusti [1, 2], Guberman [3], Takagi [4] and others paved the way for a comprehensive picture of the dynamics of the DR process. It turns out that Multichannel Quantum Defect Theory (MQDT) is the most effective theoretical framework, as far as Rydberg states are concerned. Thanks to the description of the process in terms of channels, instead of individual states, MQDT allows for a drastic reduction of the complexity of the problem. Indeed, each Rydberg series and its continuum are treated as a channel and described by a single parameter, the so-called quantum defect, if the energy is negative (bound states) or phaseshift for positive (collisional/scattering states).

However, the calculation of Rydberg states potential energy curves is still out of reach of standard quantum chemistry codes. State-of-the-art calculations are limited to the few low-lying excited states [5, 6]. The relevant quantities like quantum defects and couplings are usually extracted from these curves and extrapolated to Rydberg states in order to take into account their contributions.

In this work, we aim to turn the quantum complexity of the interplay between Rydberg and doubly-excited states into a structured picture, advancing the elucidation of the mechanisms that yield to the DR process. We show that the Halfium R-matrix method (HRM) [7] is able to address this issue and calculate Rydberg states PECs from first principles. Furthermore, an analysis within the framework of MQDT is conducted, showing the ability of the HRM method to provide a comprehensive mapping of the Rydberg manifold, from which the required ingredients for the calculation of DR cross sections and rate coefficients can be extracted.

**Corresponding author's e-mail: mourad.telmini@fst.utm.tn*
This article is based on the presentation at the Joint Conference of the 22nd International Conference on Atomic Processes in Plasmas (APiP 2025) and 1st NIFS Conference on Atomic and Molecular Processes in Plasmas.

2. The Halfium R-Matrix Method

2.1 Brief overview

The Halfium R-matrix method (HRM) combines the variational eigenchannel R-matrix theory and the Generalized Multichannel Quantum Defect Theory (GMQDT) in prolate spheroidal coordinates [7]. It was inspired by the early work of Greene and Yoo [8]. The details of the formalism can be found elsewhere [7, 9], so we will only present here a brief overview of the key points.

For each internuclear distance R, the configuration space is divided into two regions: (i) an ellipsoidal reaction volume where the two protons sit in the foci, and (ii) the remaining asymptotic zone. In the internal region, the full two-electron variational R-matrix treatment is applied and delivers a set of solutions of the Schrödinger equation, characterized by a stationary logarithmic derivative on the surface of the ellipsoid. In the asymptotic region, where only one electron can move, the radial part of the wavefunction is described within the MQDT framework, as a linear combination of one-electron Coulomb functions [10], calculated under the Halfium model approximation [7]. Specifically, the outermost electron is assumed to move in the field created by two half-positive charges placed at the foci, taking into account the partial screening of the protons by the internal electron.

By matching the internal and external solutions on the boundary surface, over a given energy grid, we obtain the short-range reaction matrix as function of both energy E and bond length R. A key requirement for the success of the calculation is the smooth dependence of the quantum defect matrix elements on E and R [7, 11].

The energy grid can encompass both the bound and the auto-ionizing spectra, enabling for a unified treatment of bound states (spectroscopy) and resonant doubly-excited states (collisions) on the same footing. The discrimination between bound and continuum channels can be processed subsequently by applying the relevant boundary conditions asymptotically.

2.2 Main applications

So far, the HRM approach has been applied to the bound states (electronic potential energy curves) and resonances (positions and widths) of ungerade ($^1\Sigma_u^+$ and $^1\Pi_u$) symmetries [7], gerade ($^1\Sigma_g^+$, $^1\Pi_g$ and $^1\Delta_g$) symmetries [11] singlet states. Then, it was extended to higher resonances [12] and $^{1,3}\Sigma^-$ states [10]. Further investigation covered high-precision ro-vibronic spectroscopy [13] and HeH^+ electronic states [14, 15].

Regarding electronic collisional processes, quantum defects and phaseshifts calculated with HRM have been used as input within the Stepwise MQDT method to produce the cross sections and rate coefficients of various processes, including vibrational and rotational excitation, as well as dissociative recombination [16].

Recently, we focused on the potential application of the HRM method in the context of full *ab initio* treatment of H_2^+ DR, which is still an open problem [17]. An update of the code allowed for the production of a new set of more precise quantum defect matrices [18].

In this paper, we go forward and present a new set of potential energy curves for the highly excited Rydberg states of H_2 with a principal quantum number $n \leq 20$. We limit ourselves to this upper bound for illustration. However, the HRM method allows for the description of an arbitrarily higher degree of excitation without significant additional computational cost.

3. Mapping Rydberg States of H_2

Although the capability of the HRM method to treat the highly excited Rydberg states was clear since the beginning, previous calculations were limited to low-lying states, where comparison with other *ab initio* data was possible. In the present work, we explicitly include these highly excited states for the first time, being confident in the quality asserted by the good agreement with the best available data at low energy. We will present the results in the case of the $^1\Sigma_g^+$ symmetry, which plays a major role in the DR process. Other symmetries are treated following the same procedure, but are not presented here.

3.1 Potential energy curves

In the $^1\Sigma_g^+$ symmetry, we consider a three-channel model with two Rydberg series converging to the ionization threshold ($1s\sigma ns\sigma$ and $1s\sigma nd\sigma$) and a doubly excited channel converging to the second ionization threshold ($2p\sigma np\sigma$). Note that we use the united-atom notation, although this notation is not rigorous for ($R \neq 0$), is only approximate for small R values and breaks down in the avoided crossing regions. However, for convenience, we will use this notation in its short version and the three channels will be referred to as $ns\sigma$, $nd\sigma$ and $np\sigma$ respectively.

Extensive calculations were conducted over a grid spanning the interval $R \in [1, 5]$ a.u., with a step of 0.01 a.u. and covering the energy range from the lowest states (n = 2, 3) up to n = 20. The size of the reaction volume is given by the scaling law of the spheroidal radius $\xi_0 = C/R + 1$, where C = 10 a.u.. The two-electron basis set was limited to about 300 functions, so the calculation time was kept low for this prototype computation (about 30 minutes per R value on a typical i5 laptop). Note that the accuracy of the calculation is expected to be improved if larger bases are used, at the cost of a longer calculation time.

The results are displayed in the following figures. In Fig. 1, we present the PECs of the electronic states. The state-of-the-art curves for the low-lying states [5] (solid blue lines) are plotted together with the HRM curves (solid green squares). The agreement between the two sets is quite good for this small-scale prototype calculation, although deviations start to show for certain states, such as $3d\sigma$ at large R values. This partial discrepancy can be attributed to the limited size of the basis and should be easily fixed with larger-scale calculations.

In Fig. 2, the Rydberg PECs around the equilibrium distance of H_2^+ ion are zoomed in. The two Rydberg series ($ns\sigma$

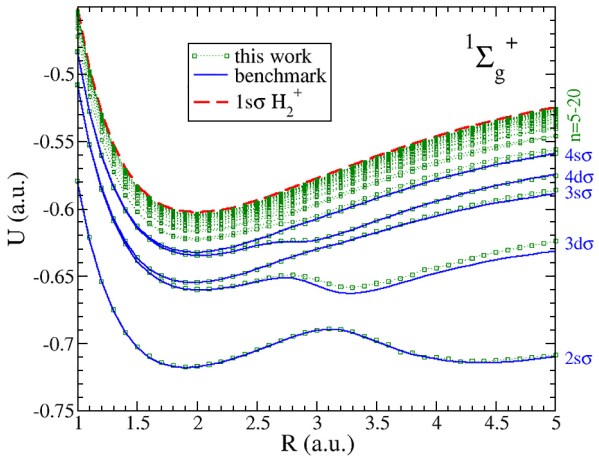

Fig. 1. Potential energy curves of the $ns\sigma$ and $nd\sigma$ (green symbols) states of the $^1\Sigma_g^+$ symmetry up to $n = 20$. The benchmark curves of Ref. [5] are plotted in blue solid lines.

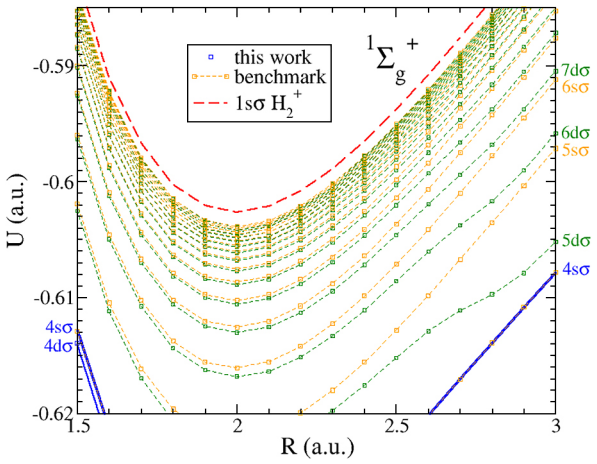

Fig. 2. Potential energy curves of the Rydberg $ns\sigma$ (orange symbols) and $nd\sigma$ (green symbols) states of the $^1\Sigma_g^+$ symmetry up to $n = 20$. The benchmark curves of $4s\sigma$ and $4d\sigma$ states Ref. [5] are plotted in blue solid lines.

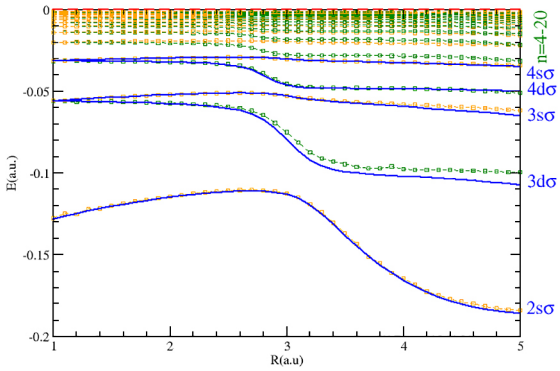

Fig. 3. Electronic energy curves of the $ns\sigma$ and $nd\sigma$ (green symbols) states of the $^1\Sigma_g^+$ symmetry up to $n = 20$. The benchmark curves extracted from of Ref. [5] are plotted in blue solid lines.

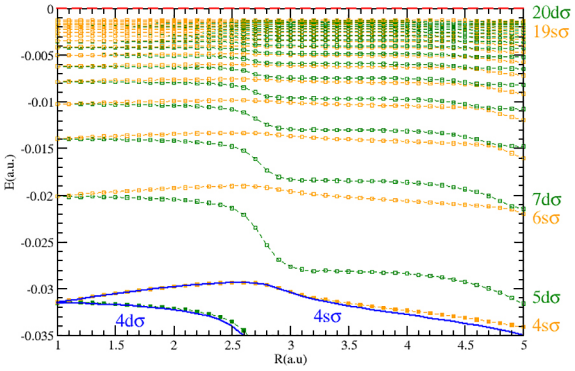

Fig. 4. Electronic energy curves of the Rydberg $ns\sigma$ (orange symbols) and $nd\sigma$ (green symbols) states of the $^1\Sigma_g^+$ symmetry up to $n = 20$. The benchmark curves of $4s\sigma$ and $4d\sigma$ states extracted from Ref. [5] are plotted in blue solid lines.

and $nd\sigma$) are easily recognized and are depicted with different colors (orange and green, respectively). Note that the unfilled gap above $n = 20$ up to the ionization threshold (red dashed line) corresponds to an energy of about 0.00125 a.u. or 34 meV. This gap can be easily reduced at will within the HRM method.

In both figures, it is quite difficult to visualize the manifold of about 40 PECs of the Rydberg states, due to the Rydberg scaling law of the energy. We rather move to the electronic energy curves.

3.2 Electronic energy curves

In Fig. 3, we display the electronic energy curves of the same states. For each electronic state $n\ell\lambda$ according to:

$$E_{n\ell\lambda}(R) = U_{n\ell\lambda}(R) - U_{ion}(R), \quad (1)$$

where $U_{n\ell\lambda}(R)$ is the potential energy of the $n\ell\lambda$ state and $U_{ion}(R)$ is the potential energy of the ground state of the H_2^+ ion.

For unperturbed Rydberg series, the electronic energy curves are expected to be flat. However, we see in Fig. 3 that the lowest states, especially $2s\sigma$, $3d\sigma$ and $4d\sigma$, are significantly distorted, illustrating in another way their well-known double-well behavior as seen in Fig. 1 (they are the EF, GK and P states respectively). Here, the $ns\sigma$ and $nd\sigma$ Rydberg series are depicted by different colors (orange and green, respectively). The large deviations from flat curves are due to the coupling of the $ns\sigma$ and $nd\sigma$ Rydberg series by the doubly excited $2p\sigma$ dissociative state.

For more clarity, the upper part of Fig. 3 is blown up in Fig. 4. It shows that the same behavior is basically duplicated for higher excited states, with strong local perturbation in the range $R = 2$–3 a.u.. Elsewhere, the curves are almost flat except around $R = 4.5$ a.u., where the second doubly-excited state $3p\sigma$ enters into play.

However, although the electronic energy curves look more convenient to illustrate the regularity and the interactions of the Rydberg series with the doubly-excited states, it is still blurring the behavior of the most highly members of the Rydberg series as we approach the ionization limit.

3.3 Effective quantum numbers

A convenient way to display the same information, within the MQDT framework, is to use the effective quantum numbers $\nu_{n\ell\lambda}(R)$ defined by (in a.u.):

$$E_{n\ell\lambda}(R) = -\frac{1}{2\nu^2_{n\ell\lambda}(R)}. \quad (2)$$

These effective quantum numbers are shown in Fig. 5. Once again, the expected behavior for the unperturbed Rydberg series includes a flat dependence with R and perfect periodicity along the Rydberg series members, whose effective quantum numbers are separated by a unit.

In Fig. 5, we see how the HRM method is able to extend the investigation of Rydberg states, far beyond the quantum chemistry methods (in solid blue at the bottom of the figure). Moreover, a regular and simple pattern appears, which allows for a insightful analysis of the spectrum. Indeed, we see a double series of Rydberg states, namely $ns\sigma$ (orange) and $nd\sigma$ (green), which are locally perturbed by the first doubly-excited state around R = 2.6 a.u. and the second doubly-excited state around R = 4.7 a.u..

On the other hand, and contrary to the potential and electronic energy curves, all the electronic states are plotted on the same footing, which is important for a global unified treatment instead of state-by-state approach.

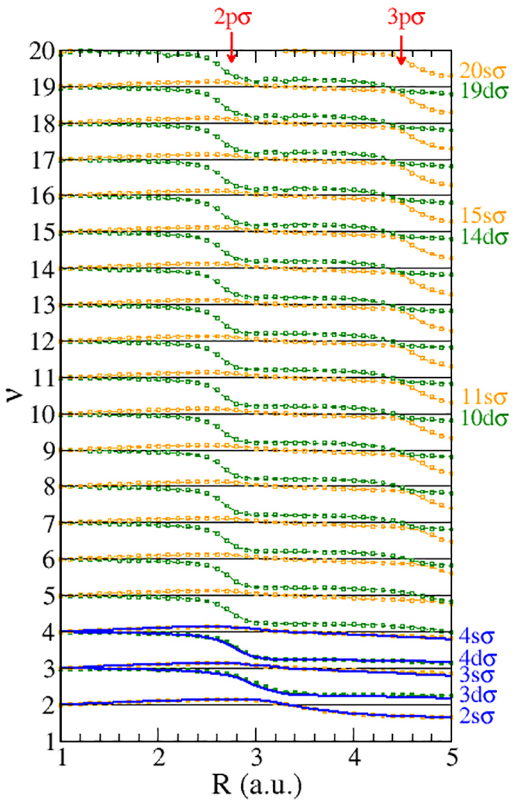

Fig. 5. Effective quantum numbers of the $ns\sigma$ and $nd\sigma$ (green symbols) states of the $^1\Sigma_g^+$ symmetry up to n = 20. The benchmark curves extracted from Ref. [5] are plotted in blue solid lines.

3.4 Quantum defects and couplings

Another compact way allowed by MQDT to display the same information, is the use of the quantum defects defined as $\mu_{n\ell\lambda}(R) = n - \nu_{n\ell\lambda}(R)$, where n is the principal quantum number, easily identified for small R in the Fig. 5, where the integer values are emphasized with horizontal black lines.

The quantum defects are displayed in Fig. 6 instead of the effective quantum numbers. As a consequence, the information contained in Fig. 5 is synthesized thanks to the scaling laws of MQDT and we see in Fig. 6 two well-separated bundles of curves related to $ns\sigma$ (orange) and $nd\sigma$ (green) channels, while benchmark values, for the lowest states, are plotted in solid blue line.

As stated earlier, benchmark curves are usually used as a starting point for the MQDT treatment, assuming in general that they can be extrapolated to highly-excited Rydberg states. Our results constitute an alternative to this approach, by providing *ab initio* quantum defects for highly excited states. Moreover, HRM quantum defects are energy-dependent by definition, avoiding any need of *ad hoc* assumptions for their energy dependence.

Indeed, the present approach delivers the *ab initio* values of the quantum defects in both channels, from which quasi-diabatic quantum defects and couplings with the $np\sigma$ doubly-excited channel can be extracted, without any further adjustment or extrapolation. These curves can be used as reliable data for the implementation of the stepwise MQDT approach for a better estimation of the cross sections and rate coefficients. Moreover, our approach can be extended to include the second doubly-excited state, which enters into play

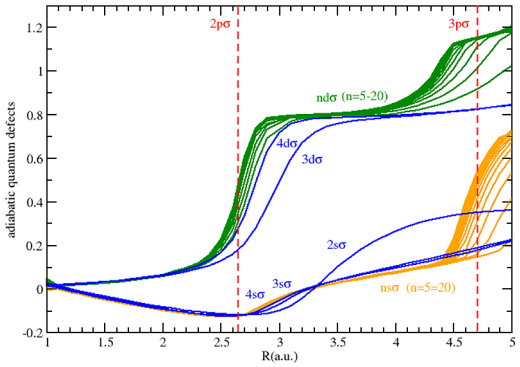

Fig. 6. Quantum defects curves of the $ns\sigma$ (orange) and $nd\sigma$ (green) states of the $^1\Sigma_g^+$ symmetry up to n = 20. The benchmark curves extracted from Ref. [5] are plotted in dashed blue lines. The two dashed vertical lines depict the internuclear distances at which the PEC of first ($2p\sigma$) and the second ($3p\sigma$) excited state cross the ionization threshold.

for $R \geq 4$ a.u., by using the same recipe. Furthermore, we expect similar behavior at larger R values where more and more doubly-excited states could be taken into account, improving the calculation of the relevant collisional quantities.

In addition to quantum defects, the couplings between the Rydberg channels and the doubly-excited $np\sigma$ states are key quantities for the stepwise MQDT computation. These couplings are directly related to the off-diagonal elements of the quantum defect matrix. They are generally extracted from the widths of the $np\sigma$ doubly excited states resonances above

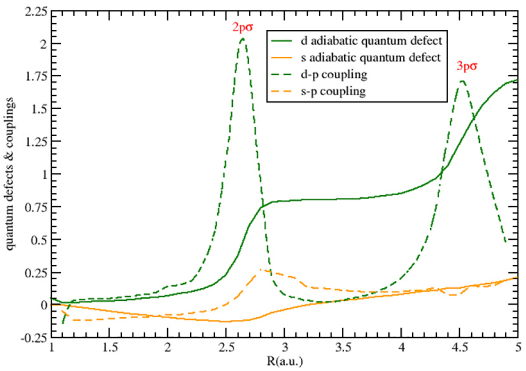

Fig. 7. Quantum defects and couplings with doubly-excited states for the *d*-wave and *s*-wave extracted from Fig. 6 for $n = 18$.

the threshold and are extrapolated below the ionization threshold. A major limitation of this method is that the doubly-excited states lie above the ionization threshold only at small R values. For example, the first resonance $2p\sigma$ crosses the threshold at $R = 2.6$ a.u., while the second resonance $3p\sigma$ crosses the threshold at $R = 4.5$ a.u.. Beyond these values, the couplings are still visible in the double-well structures dug into the PECs of some states (see Fig. 1). However, their direct extraction from the PECs is not easy and quasi-diabatization procedures are used to address this issue.

In the present approach, the couplings can be directly extracted from Fig. 6. In fact, the sharp variations of the $nd\sigma$ channel around $R = 2.7$ and 4.5 a.u. are directly caused by the coupling of this channel and the two lowest $2p\sigma$ and $3p\sigma$ doubly excited states. The idea is to transform the adiabatic quantum defects, shown in Fig. 7 to a quasi-diabatic set of quantum defects and couplings.

Indeed, in Fig. 7, the derivative of the quantum defects with respect to the internuclear distance R (dashed orange and green curves), are plotted together with the quantum defects (solid orange and green curves), for $n = 18$. The dashed curves present Breit-Wigner type profiles, which are directly related to the couplings between $ns\sigma$ and $nd\sigma$ channels with $np\sigma$ doubly excited states. These couplings can be used as a starting point in the quasi-diabatization procedure to determine the quasi-diabatic quantum defects in each channel. In a further step, the new set could be incorporated into the stepwise MQDT formalism after a relevant rescaling of the couplings with those extracted from resonance widths above the ionization threshold.

Moreover, the procedure can be easily extended to incorporate higher doubly excited states, by performing the HRM treatment for larger internuclear distances. Other channels can be introduced as well, either as Rydberg series with higher ℓ ($ng\sigma$ channel, …) or doubly excited resonances ($nf\sigma$ resonances, …). Also, the energy dependence of both quantum defects and couplings can be added to the stepwise MQDT method toolbox. Actually, the HRM method opens the door to several improvements and more comprehensive approach within the stepwise MQDT method, which should result in improved calculations of the H_2^+ Dissociative Recombination cross sections and rate coefficients.

4. Conclusion

In this paper, we have presented a series of calculations of ab initio Potential Energy Curves of the Rydberg states of the $^1\Sigma_g^+$ symmetry of H_2, obtained with the HRM method. We have illustrated the ability of the HRM method to fill the gap toward highly excited Rydberg states up to n = 20. Moreover, by transforming the PECs into electronic energy curves, then to effective quantum numbers curves, we have shown that regular patterns resulting from the coupling of the Rydberg series with doubly-excited states can be displayed in a comprehensive way.

A further step, consisting in moving from the effective quantum numbers to the quantum defects, allows for the reduction of the same information to a compact set of well-separated bundles characterizing each Rydberg series and its coupling with the doubly excited states. The shape of the quantum defects is suitable for the extraction of the intra-channel quantum defects and the inter-channel couplings which are the required ingredients for the calculation of the cross sections and rate coefficients with the stepwise MQDT approach.

In summary, HRM ab initio quantum defects for highly-excited Rydberg states of H_2 are proposed as an alternative to the sets obtained by extrapolation from the low-lying states and used in the stepwise MQDT method. This procedure will be implemented in the case of ($e + H_2^+$) and ($e + HD^+$) collisions and reported subsequently.

Acknowledgments

Part of this work was started at the Department of Physics and Astronomy of Purdue University. M.T. thanks Prof. Chris H. Greene for his invitation and hospitality. The work of C.H.G. was supported by the U.S. Department of Energy, Office of Science, Office of Basic Energy Sciences, Award No. SC0010545.

[1] A. Giusti, J. Phys. B: At. Mol. Opt. Phys. **13**, 3867 (1980).
[2] I.F. Schneider *et al.*, J. Phys. B: At. Mol. Phys. **24**, L289 (1991).
[3] S.L. Guberman, J. Chem. Phys. **78**, 1404 (1983).
[4] H.J. Takagi and H. Nakamura, J. Phys. B. **13**, 2619 (1980).
[5] M. Silkowski *et al.*, Adv. Quant. Chem. **83**, 255 (2021).
[6] H. Nakashima and H. Nakatsuji, J. Chem. Phys. **149**, 244116 (2018).
[7] M. Telmini and Ch. Jungen, Phys. Rev. A **68**, 062704 (2003).
[8] C.H. Greene and B. Yoo, J. Phys. Chem. **99**, 1711 (1995).
[9] F. Argoubi *et al.*, Phys. Rev. A **83**, 052504 (2011).
[10] R. Guérout *et al.*, Phys. Rev. A **79**, 042717 (2009).
[11] S. Bezzaouia *et al.*, Phys. Rev. A **70**, 012713 (2004).
[12] H. Oueslati *et al.*, Mol. Phys. **104**, 187 (2006).
[13] H. Oueslati *et al.*, Phys. Rev. A **89**, 032501 (2014).
[14] I. Bouhali *et al.*, EPJ Web of Conferences **84**, 04004 (2015).
[15] I. Bouhali *et al.*, Phys. Rev. A **94**, 022516 (2016).
[16] O. Motapon *et al.*, Phys. Rev. A **90**, 012706 (2014).
[17] D. Hvizdos *et al.*, Phys. Rev. A **111**, 012805 (2025).
[18] D. Hvizdos *et al.* (private communication).